DEVELOPING REGIONALIZED MODELS OF LITHOSPHERIC THICKNESS AND VELOCITY STRUCTURE ACROSS EURASIA AND THE MIDDLE EAST FROM JOINTLY INVERTING P-WAVE AND S-WAVE RECEIVER FUNCTIONS WITH RAYLEIGH WAVE GROUP AND PHASE VELOCITIES

Jordi Julià[1], Andrew A. Nyblade[1], Arthur J. Rodgers[2], and Eric Matzel[2]

Penn State University[1] and Lawrence Livermore National Laboratory[2]

Sponsored by National Nuclear Security Administration

Award Nos. DE-AC52-09NA29322[1] and LL09-BAA09-13-NDD03[2]
Proposal No. BAA09-13

ABSTRACT

The main goal of this project is to develop regionalized models of lithospheric velocity structure for a wide variety of tectonic regions throughout Eurasia and the Middle East. We expect the regionalized models will improve the ability of the National Nuclear Security Administration (NNSA) labs to predict travel times for local and regional phases, such as Pg, Pn, Sn and Lg, as well as travel times for body waves at upper-mantle triplication distances in both seismic and aseismic regions. The models have been developed following a two-step approach: (i) first, one-dimensional (1D) velocity models for select broadband stations are obtained by jointly inverting P- and S-wave receiver functions and fundamental-mode group and phase dispersion velocities, and (ii) regionalized velocity models are then constructed by combining the 1D joint inversion models within each tectonic region and validated through regional waveform modeling. The velocity models thus obtained will also help inform and strengthen ongoing and future efforts within the NNSA labs to develop 3D velocity models for Eurasia and the Middle East, and will assist in obtaining model-based predictions where no empirical data are available and for improving locations from sparse networks.

During the first year of this project, we have developed 1D velocity models for 54 locations in Europe and 10 locations in the Middle East. Receiver functions were computed from teleseismic P- and S-waveforms recorded at open broadband stations and archived at the Data Management Center of the Incorporated Research Institutes for Seismology (IRIS-DMS), while dispersion velocities were obtained from an independent surface-wave tomography study for Eurasia and North Africa. Due to a combination of short recording time-windows and inefficient recording of teleseismic S-waves, some locations in Western Europe did not yield reliable S-wave receiver function estimates. To improve coverage in the Middle East, we also computed receiver functions at broadband stations from the Israel National Seismic Network, made available through the GEOFON program. The joint inversion models reveal important differences in lithospheric structure between the cratonic regions of Eastern Europe and the tectonic regions of Western Europe and the Middle East. Lithospheric structure in Eastern Europe is generally characterized by a gradual increase in seismic velocity with depth and no sharp velocity decrease down to maximum inversion depths of ~250 km. In contrast, the lithospheric mantle in Western Europe and the Middle East displays relatively sharp velocity variations, defining low-velocity zones of varying thicknesses, depths, and minimum velocities.

We are now combining the 1D velocity models obtained from the joint inversion of P- and S-wave receiver functions and dispersion velocities to construct regionalized velocity models for the tectonic regions of Europe and the Middle East. We have also identified a number of regional events in the Lawrence Livermore National Laboratory (LLNL) Ground-Based Nuclear Explosion Monitoring (GNEM) Seismic Research Database with well-determined source parameters and broadband recordings with ray-paths predominately in a single tectonic region (pure path propagation) to validate the regionalized velocity models. During the next year, we will continue the development of 1D velocity models from the joint inversion of receiver functions and dispersion velocities at open broadband stations in Asia and the construction and validation of regionalized velocity models for the corresponding tectonic regions.

OBJECTIVES

The main objective of this project is to develop new velocity models for Eurasia and the Middle East that improve the ability of the NNSA labs to predict travel times for local and regional phases, such as Pg, Pn, Sn and Lg, as well as travel times for body waves at upper-mantle triplication distances in both seismic and aseismic regions. The models are being developed by combining multiple seismic datasets through a joint inversion scheme that integrates the complementary constraints conveyed by each dataset while bridging resolution gaps among them. We are placing special emphasis on constraining the velocity structure of the lithospheric mantle, the thickness of the lithosphere, and the structure of the low-velocity zone under the lithosphere, as models that parameterize the upper mantle as infinitely thick cannot accurately model rays that penetrate below the lithosphere.

The seismic datasets contributing to the new velocity models include P-wave receiver functions (PRFs), S-wave receiver functions (SRFs), Rayleigh-wave group velocities, and Rayleigh-wave phase velocities. All datasets are sensitive to S-wave velocity structure, but are sensitive to complementary aspects of that structure. PRFs constrain detailed crust and uppermost mantle structure through S-P travel times and velocity contrast across discontinuities; SRFs constrain detailed lithospheric mantle structure, including lithospheric thickness, through P-S travel times and velocity contrasts across discontinuities; and surface-wave dispersion velocities constrain large-scale average velocity structure at frequency-dependent depth ranges across the crust and upper mantle. The combination produces S-wave velocity-depth profiles where the high-resolution details constrained by the receiver functions are superimposed on a background velocity model constrained by the dispersion velocities (Julià et al., 2000).

The velocity models are being developed following a two-step approach. In the first step, PRFs and SRFs obtained at individual broadband stations are jointly inverted with tomographic Rayleigh-wave dispersion velocities from independent surface-wave studies to develop local 1D velocity-depth profiles at each location. In the second step, the local 1D models are combined within geologic/tectonic terrain defined in published terrain maps, such as the WENA and UNIFIED models of Pasyanos et al. (2003, 2004), to produce regionalized velocity models of the crust and upper mantle for each terrain. The regionalized models represent the average velocity structure within the corresponding tectonic/geologic region.

The regionalized models are evaluated through 1-D waveform modeling for events with well-determined source parameters (depth, seismic moment, and focal mechanism) and broadband recordings with ray paths predominately in a single tectonic/geologic region. The model validation effort focuses on regions where there is good event-station coverage (i.e., pure path propagation within a region) over a range of local and regional distances and also includes an investigation of the misfits between data and synthetics to understand how the regionalized models need to be perturbed to improve the fits in phase and amplitude.

In addition to improving the ability of the NNSA labs to predict local and regional phase travel times in Eurasia and the Middle East, the regionalized velocity models will also help inform and strengthen ongoing and future efforts to develop 3-D velocity models for Eurasia and the Middle East. What is also important is that the new velocity models will assist in obtaining model-based predictions where no empirical data are available (e.g., Flanagan et al., 2006) and in improving locations from sparse networks (e.g., Schultz et al., 1998; Myers and Schultz, 2000).

RESEARCH ACCOMPLISHED

During the first year of application of this project, we have developed local 1D models for open broadband stations in Europe and the Middle East (Figure 1). We have concentrated on permanent broadband stations with operating times over 5 years in order to develop robust receiver function averages and to be able to inspect for azimuthal variations around the station. Using large datasets is especially important for obtaining reliable SRF estimates, as events must be within epicentral distance ranges that are narrower than those for PRFs (Wilson et al., 2006), and the deconvolution process is more unstable.

Data Gathering

Broadband seismic waveforms for computation of PRFs and SRFs were downloaded from the IRIS-DMC using the SOD utility (Owens et al., 2004) for all open broadband stations in Europe and the Middle East. For PRFs we selected events with magnitudes above 5.5 and sources at epicentral distances between 30^o and 90^o, and events with magnitudes above 6.0 and sources at epicentral distances between 60^o and 85^o were considered for SRFs. These

distance ranges keep the teleseismic P- or S-wave from interfering with other teleseismic arrivals and are commonly utilized for receiver function computation (e.g., Julià et al., 2008; Hansen et al., 2007).

The majority of the stations archived at the IRIS-DMC are contributed from temporary IRIS PASSCAL-type deployments, with short operation times, and concentrate on small geologic/tectonic regions, mostly in Europe. As a result, the station coverage of Eurasia and the Middle East is quite uneven and can be quite sparse in some areas. This problem is especially critical for the Middle East, where only 6 permanent broadband stations are available at the IRIS-DMC. To alleviate this situation, we downloaded data from the GEOFON data center for four additional open broadband stations operated by the Israeli Seismic Network. Overall, a dataset of 88,530 P-waveforms and 9,279 S-waveforms recorded at 64 broadband stations was assembled.

Fundamental-mode, Rayleigh-wave group velocities in Europe and the Middle East were obtained from the surface-wave tomography study of Pasyanos (2005). In that study, local dispersion curves were obtained for Eurasia, the Middle East, and North Africa by inverting fundamental-mode, Rayleigh-wave group velocities measured along more than 30,000 source-station paths with a conjugate-gradient method with variable smoothness. The resulting surface-wave tomography maps highlight lateral variations across the region for periods between 7 and 100 s, with a resolution approaching 1º.

Regional events with ray paths contained within terrains defined in the UNIFIED and WENA models are now being identified for Europe and the Middle East. These events will be utilized to evaluate the average velocity models that will be developed for the geologic/tectonic terrains from the local 1D models.

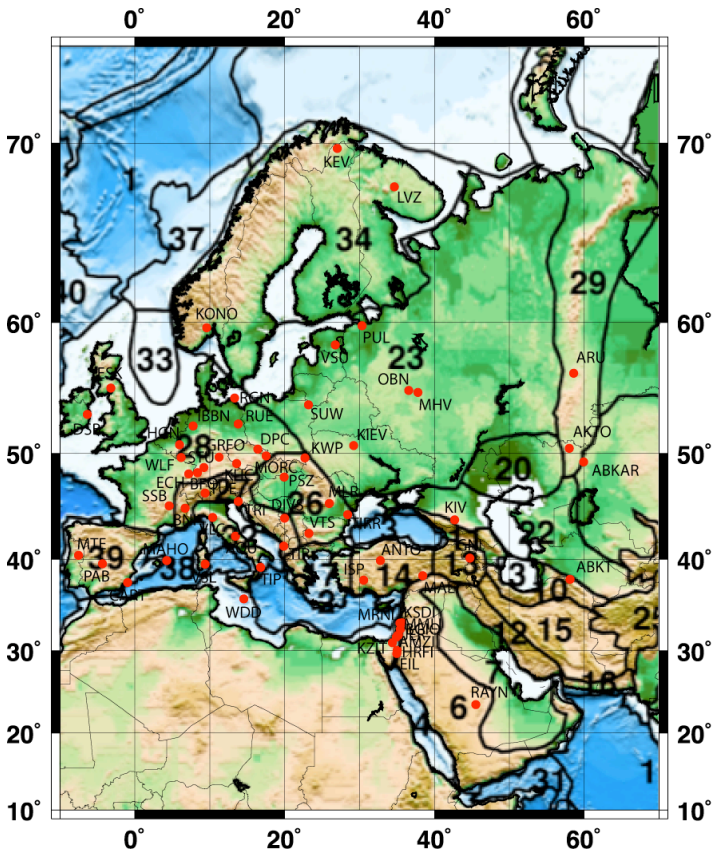

Figure 1. Topographic map of Europe and the Middle East showing the open broadband stations analyzed so far and the WENA/UNIFIED regions as defined in Pasyanos et al. (2003; 2004)

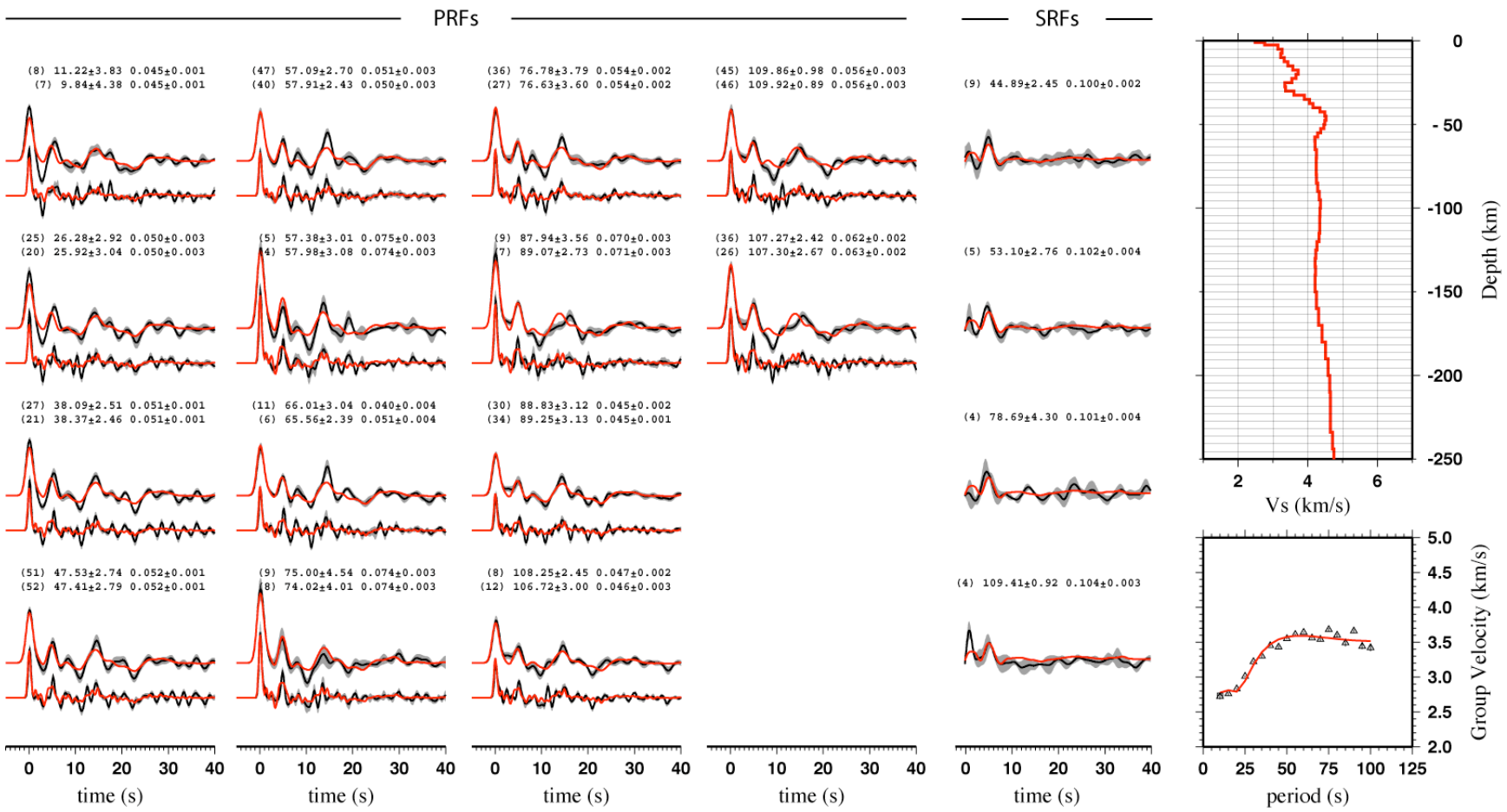

Figure 2. Joint inversion results for station MALT, in southern Turkey. The left panels are the observed (black) and predicted (red) PRFs at two overlapping frequency bands of fc<0.5 Hz and fc<1.2 Hz, the middle panels are the observed (black) and predicted (red) SRFs. The upper-right panel is the inverted model, and the bottom-right panel are the observed (triangles) and predicted (red line) dispersion velocities. The grey shadows surrounding the observed PRFs and SRFs and the vertical lines across the dispersion measurements are the 1σ-confidence bounds. The number of waveforms (n), average back-azimuth and standard deviation in deg (baz±1σbaz), average ray-parameter and standard deviation in s/km (rayp±1σr) is indicated on top of each receiver function panel.

Receiver Function Computation

Computation of PRFs was performed in the ZRT system by deconvolving the vertical component of the teleseismic P-waveforms from the corresponding radial component (e.g., Langston, 1979). Prior to deconvolution, the waveforms were windowed 10 s before and 110 s after the teleseismic P-wave arrival, detrended, tapered, and decimated to 10 samples per second (s.p.s.). The waveforms were low-pass filtered at 8 Hz before decimation to avoid aliasing and high-pass filtered above 0.05 Hz to remove low-frequency noise. PRFs were computed at two overlapping frequency bands of $f < 1.2$ Hz and $f < 0.5$ Hz. The combination of high and low frequencies provides constraints on velocity structure at different wavelengths and helps discriminate sharp boundaries from gradational transitions (Owens and Zandt, 1985; Julià, 2007). The deconvolution operation was applied using the iterative, time-domain deconvolution of Ligorría and Ammon (1999), with 500 iterations.

Transverse PRFs were also obtained by deconvolving the vertical component of the teleseisimc P-waveforms from the corresponding transverse component. Transverse PRFs are not used to constrain our local 1D models, but they offer a good dimensionality check on the structure under the station. For 1D structures the transverse receiver function should be identically zero; if the signal in the transverse PRF is comparable to that of the radial PRF, the model is not 1D (or anisotropic), and modeling of the radial PRF cannot be achieved through simple 1D velocity models.

On the other hand, SRFs were obtained in the local ray-coordinate (LQT) system by deconvolving the SV component of the teleseismic S-waveforms from the corresponding P component (Farra and Vinnik, 2000). The waveforms were windowed 100 s before and 12 s after the teleseismic S-wave arrival, detrended, tapered, and decimated down to 10 s.p.s. Similar to PRFs, the waveforms were low-pass filtered at 8 Hz to avoid aliasing and high-pass filtered above 0.05 Hz. Following standard practices in SRF computation (e.g., Hansen et al., 2007), the waveforms were time-reversed and polarity-flipped. Again, the deconvolution operation was performed through the iterative, time-domain deconvolution of Ligorría and Ammon (1999), with 500 iterations.

In general, we observed that the deconvolution process for S-waveforms is more unstable than for P-waveforms. We attribute this instability to the fact that Sp conversions happen within the coda of the teleseismic P-wave and to the difficulty in isolating the teleseismic S-wave pulse from other teleseismic phases (SKS, SKKS, SP) and from crustal reverberations. Given the relatively narrow range of epicentral distances suitable for SRF computation (60^o to 85^o), we decided to focus on stations with long operating times to obtain reliable SRF averages and robustly constrain lithospheric and sublithospheric structure.

A first-pass quality control was applied to the computed PRFs and SRFs by requiring that the convolution of the receiver functions with the corresponding vertical waveforms (PRFs) or SV waveforms (SRFs) reproduced 85% or more of the original radial and P-waveforms, respectively. The remaining receiver functions were then further inspected for visual stability and waveform consistency. Overall, we obtained 15,517 high-frequency PRFs ($f < 1.2$ Hz), 14,244 low-frequency PRFs ($f < 0.5$ Hz), and 965 SRFs ($f < 0.5$ Hz) for the selected 64 broadband stations in Eurasia and the Middle East.

Local 1D Velocity Models

Local 1D velocity models have been developed for Europe and the Middle East by jointly inverting PRFs and SRFs with Rayleigh-wave group velocities from the tomographic study of Pasyanos (2005) for S-wave velocity structure. Rayleigh-wave phase velocities will be added at a later stage. The velocity models are parameterized as a stack of thin layers down to ~400-km depth, with layer thicknesses ranging from 1.0 km for sedimentary structures, to 2.5 km for the crust and uppermost mantle (down to 60-km depth), 5.0 km for lithospheric mantle (down to 150-km depth), and 10.0 km for deeper structures. Layer thicknesses and Vp/Vs ratios are fixed for each layer during the inversion process, and densities are obtained from P-wave velocities through an empirical relationship (Berteussen, 1977). The models are parameterized down to ~400 km depth but only structure for the top 250 km is inverted for. Seismic velocities for layers deeper than 400 km are fixed to PREM values (Dziewonski and Anderson, 1981) in order to account for partial sensitivity of the long-period dispersion velocities to deep structure (Julià et al, 2003).

The joint inversion procedure utilized follows the iterative, linearized approach of Julià et al. (2003). The approach is described by the following system of equations:

$$\begin{bmatrix} \sqrt{\frac{p}{w_s^2}}\, D_s \\ \sqrt{\frac{q}{w_b^2}}\, D_b \\ \sigma\Delta \\ A \end{bmatrix} \vec{m} = \begin{bmatrix} \sqrt{\frac{p}{w_s^2}}\, \vec{r}_s \\ \sqrt{\frac{q}{w_b^2}}\, \vec{r}_b \\ \vec{0} \\ A\,\vec{m}_a \end{bmatrix} + \begin{bmatrix} \sqrt{\frac{p}{w_s^2}}\, D_s \\ \sqrt{\frac{q}{w_b^2}}\, D_b \\ \vec{0} \\ \vec{0} \end{bmatrix} \vec{m}_o$$

where D_s and D_b are partial derivative matrices for the dispersion and the receiver function estimates, respectively, r_s and r_b are the corresponding vectors of residuals, w_s^2 and w_b^2 are weights that equalize the datasets, the vector m contains the velocities of fixed thickness layers overlying a half-space, and m_0 contains an initial estimate for the velocities. The matrix Δ constructs the second difference model and makes the resulting profiles vary smoothly, and the diagonal matrix W contains constraint weights to the *a priori* velocity values m_a. The influence factor p controls the trade-off between fitting the receiver functions and the dispersion curves, and the smoothness parameter σ controls the trade-off between fitting the data and model smoothness. The values of these parameters are determined empirically by performing suites of inversions. The parameter $q = 1-p$, with $0 \leq p \leq 1$, so that $p = 0$ means inverting receiver function data only and $p = 1$ means inverting dispersion data only. The weights w_s^2 and w_b^2 are computed as $N\sigma^2$, where N is the number of data points and σ^2 is the variance of the observations.

The development of the 1D local models is illustrated in Figure 2, which displays the joint inversion results for the GEOFON station MALT in southern Turkey. The observations consist of 28 PRF averages (14 at frequencies < 1.2 Hz; 14 at frequencies < 0.5 Hz), 4 SRF averages (at frequencies < 0.5 Hz), and 1 dispersion curve (fundamental-mode Rayleigh-wave group velocity) extracted from the tomographic cell in Pasyanos (2005) enclosing the station. The different PRF and SRF averages are point-to-point stacks from teleseismic waves approaching the recording station from different directions and at different incidence angles. The starting model consisted of a simple gradational crust overlying PREM, which converged to a stable solution after six iterations with the aid of depth-dependent smoothing constraints on the profiles ($\sigma = 0$ .5 down to 100 km; $\sigma = 1.0$ underneath).

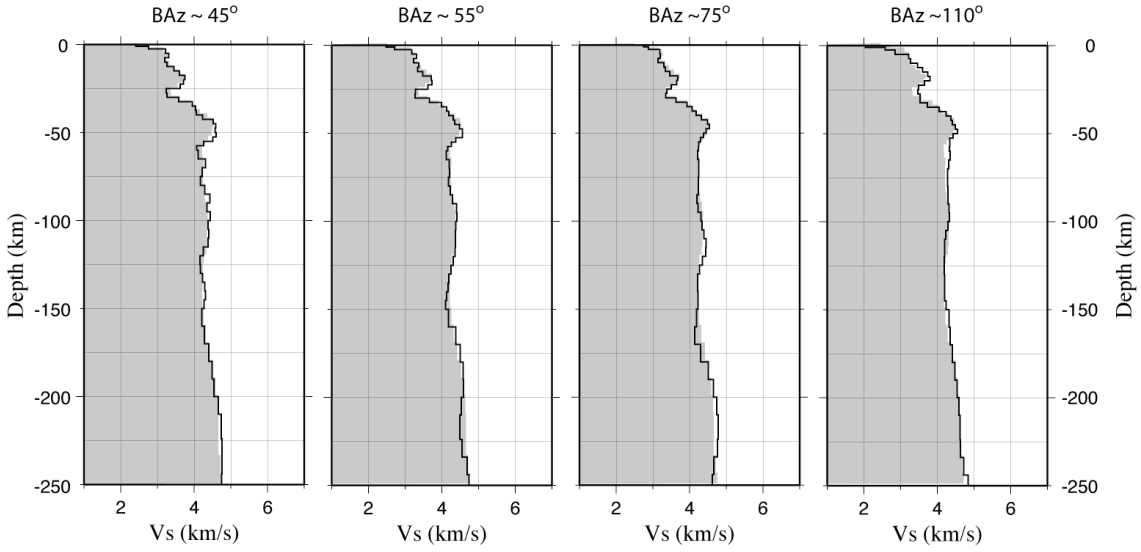

Figure 3. Velocity models corresponding to 4 separate joint inversions using PRF and SRF averages sampling at ~45°, ~55°, ~75°, and ~110° from the recording stations. The dispersion velocities constraining the velocity models were the same. The grey shade is the average velocity model displayed in Figure 2.

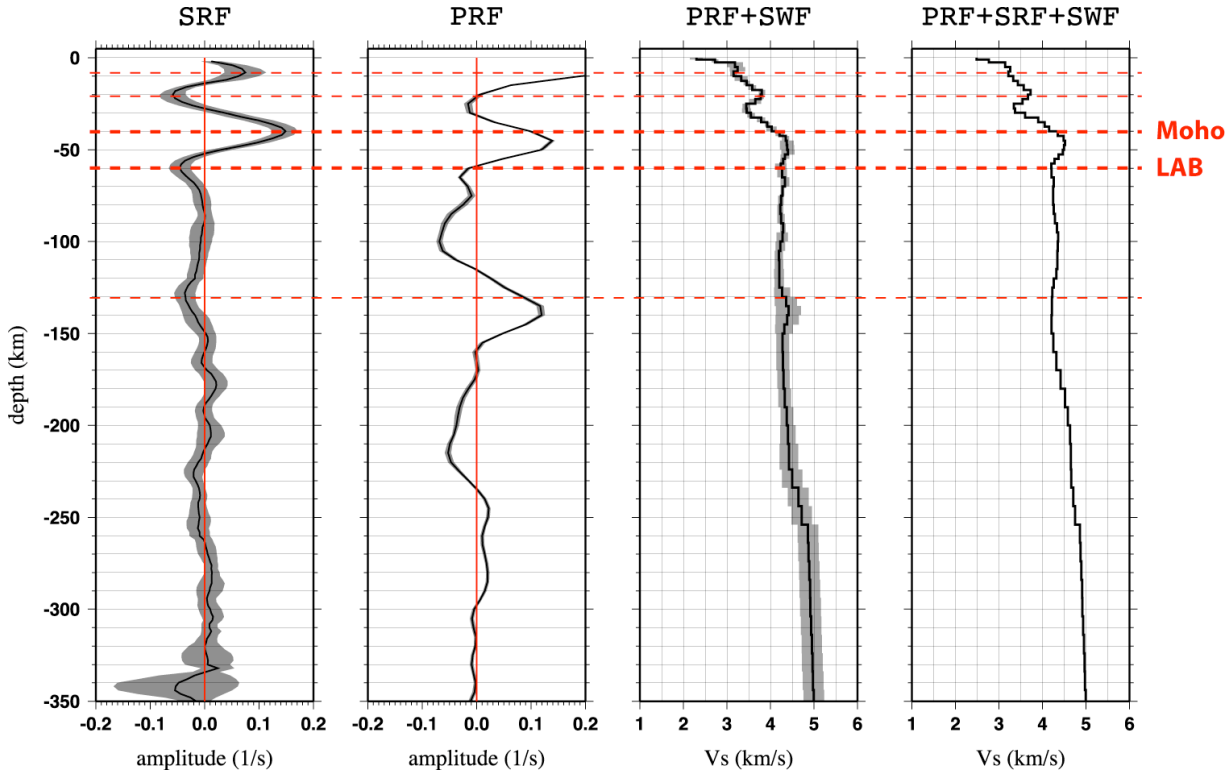

Figure 4. Correlation between joint inversion models with and without SRF constraints and depth-migrated PRF and SRF stacks for station MALT. The grey band in the SRF panel denotes the 1σ-confidence bounds for the SRF stack, and the grey band in the PRF+SRF panel denotes the 1σ-confidence bounds for the velocity model. The red dashed lines mark the statistically significant peaks and troughs in the SRFs.

The comparison between observations and predictions is excellent for the dispersion velocities, but some discrepancies are observed for the receiver functions. These discrepancies are the result of azimuthal variations in velocity structure around the station. The main features in all datasets, nonetheless, are satisfactorily accounted for, and the resulting velocity model can be regarded as a representative average. The main features of the velocity-depth profile for station MALT include (i) a ~40-km-thick crust, (ii) a low-velocity zone centered at ~25-km depth, (iii) a thin upper mantle lid (10–15 km thick), (iv) a shallow LAB (at ~55-km depth), and (v) a gradual velocity increase between 150- and 180-km depth back to PREM values. In order to check the robustness of those features and also to assess the degree of azimuthal heterogeneity around the station, we performed separate joint inversions for select PRF and SRF averages (Figure 3). The resulting velocity models show that, although the details may vary among the models, all the features are required to explain each of the separate inversions.

It is important to realize that the structure in the lithospheric mantle is strongly influenced by the constraints conveyed by the SRF average. This is illustrated in Figure 4, which displays the joint inversion model in Figure 2, along with depth-migrated PRF and SRF stacks (frequencies < 0.5 Hz) and the velocity model resulting from jointly inverting the PRF averages with the dispersion velocities (without the SRF contribution). The figure shows that the velocity decrease at 55-km depth correlates with the downswing (S-to-P conversion) in the SRF average at similar depths but that it was not required to explain the PRF average. It also shows that the velocity increase at ~130-km depth observed in the joint inversion model with no SRF data is removed with the addition of this dataset. Also, note that the crustal structure does not differ much with and without the contribution of the SRF data.

Some stations did not yield enough SRF waveforms to compute reliable SRF averages; therefore, the velocity models were developed without SRF constraints. This can introduce artifacts in the lithospheric structure due to partial modeling of crustal reverberations with Ps conversions in the mantle. These models will be down-weighted during the development of the average regional velocity models for the geologic/tectonic terrains.

Regional Velocity Models

We are now developing average velocity models for the WENA/UNIFIED terrains displayed in Figure 1 from the local 1D velocity models developed so far for Europe and the Middle East. Figure 5 displays the velocity models for region No. 23, approximately coinciding with Eastern Europe. The models display significant variation in crustal structures but a more-or less-homogeneous lithospheric mantle characterized by the absence of a clear LAB (down to the maximum resolvable depth of ~250 km).

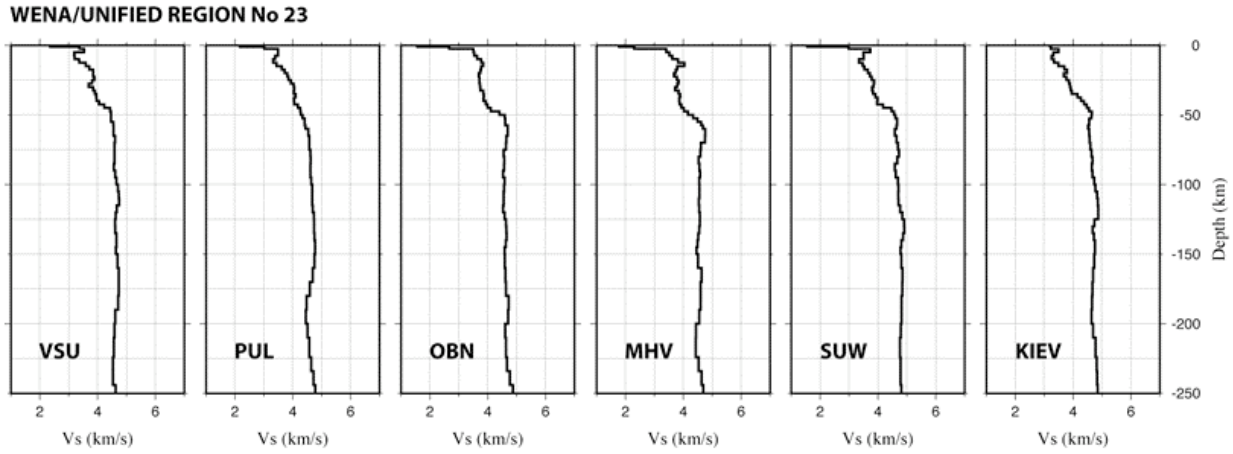

Figure 5. Local 1D velocity models for all the stations enclosed in the WENA/UNIFIED region No. 23 (Figure 1). Two of the models, PUL and KIEV, did not produce stable SRFs and were constrained from PRFs and dispersion only. Note that all the models constrained with SRF data are characterized by the absence of a LAB down to 250 km depth.

CONCLUSIONS AND RECOMMENDATIONS

We have developed local 1D velocity models for 64 permanent broadband stations in Europe and the Middle East by jointly inverting PRFs, SRFs, and fundamental-model, Rayleigh-wave group velocities. The data for PRF and SRF computation was downloaded from open stations at the IRIS DMC (60) and GEOFON (4) data archives, and the group velocities were obtained from the independent tomographic study of Pasyanos (2005). The inclusion of SRF waveforms into the joint inversion has proven critical to robustly constrain lithospheric thickness and lithospheric velocities.

The sampling of the WENA/UNIFIED tectonic models provided by the permanent broadband stations archived at the IRIS-DMC is quite uneven. Station coverage is best in the terrains of Western Europe, and it degrades towards Eastern Europe and the Middle East. Two possibilities for alleviating this situation include (i) obtaining data from permanent broadband stations freely available at other data centers (e.g., GEOFON, ORFEUS) and (ii) developing velocity models from temporary networks in terrains where the sampling from permanent stations is poor. As mentioned above, additional station coverage for the Middle East has been obtained from the Israeli Seismic Network through the GEOFON data center. Due to the larger instability of the deconvolution process in SRF computation, developing local 1D velocity models from temporary deployments will require combining data from several stations.

Stations in Western Europe are somewhat more inefficient in recording teleseismic S-waves than stations in Eastern Europe and the Middle East. As a result, a number of velocity models had to be developed with no SRF constraints or with less-robust SRF averages. To augment the dataset, we will investigate the use of SKS waves for SRF computation, which has shown some promise in other regions such as South Africa (Wittlinger and Farra, 2007) or South America (Heit et al., 2007).

ACKNOWLEDGEMENT

We would like to thank the IRIS-DMC and GEOFON data center for their role in the archiving and distribution of seismic data utilized for this project.

REFERENCES

Berteussen, K. A. (1977). Moho depth determinations based on spectral ratio analysis of NORSAR long-period P-waves, *Phys. Earth Planet. Inter*. 31: 313–326.

Dziewonsky, A. M. and D. L. Anderson (1981). Preliminary reference earth model, *Phys. Earth and Planet. Inter.* 25: 297–356.

Farra, V. and L. Vinnik (2000). Upper mantle stratification by P and S receiver functions, *Geophys. J. Int.* 141: 699–712.

Flanagan, M., S. Myers, and K. Koper (2006). Regional travel-time uncertainty and seismic location improvement using a three-dimensional a priori velocity model, *EOS Trans. AGU* 87: S31B–0194.

Hansen, S., A. Rodgers, S. Schwartz, and A. Al-Amri (2007). Imaging ruptured lithosphere beneath the Red Sea and Arabian Peninsula, *Earth Planet. Sci. Lett.* 259: 256–265.

Heit, B., F. Sodoudi, X. Yuan, M. Bianchi, and R. Kind (2007). An S receiver function analysis of the lithospheric structure in South America, *Geophys. Res. Lett.* 34: L143078, doi:10.1029/2007GL030317.

Julià, J. (2007). Constraining velocity and density contrasts across the crust-mantle boundary with receiver function amplitudes, *Geophys. J. Int.* 171: 286–301.

Julià, J., C. J. Ammon, R. B. Herrmann, and A. M. Correig (2000). Joint inversion of receiver function and surface wave dispersion observations, *Geophys. J. Int.* 143: 99–112.

Julià, J., C. Ammon, and R. Herrmann (2003). Lithospheric structure of the Arabian Shield from the joint inversion of receiver functions and surface-wave group velocities, *Tectonophysics* 371: 1–21.

Julià, J., M. Assumpção, and M. Rocha (2008). Deep crustal structure of the Paraná Basin from receiver functions and Rayleigh-wave dispersion: Evidence for a fragmented cratonic root, *J. Geophys. Res*. 13: B08318, doi:10.1029/2007JB005374.

Langston, C. (1979). Structure under Mount Rainier, Washington, inferred from teleseismic body waves, *J. Geophys. Res.* 84: 4749–4762.

Ligorría, J. and C. Ammon (1999). Poisson's ratio variations of the crust beneath North America, *Seism. Res. Lett.* 89: 1395–1400.

Myers, S. and C. Schultz (2000). Improving sparse network seismic location with Bayesian kriging and teleseismically constrained calibration events, *Bull. Seis. Soc. Am*. 90: 199–211.

Owens, T. J., H. P. Crotwell, C. Groves, and P. Oliver-Paul (2004). Standing order for data, *Seism. Res. Lett.* 75: 515–520.

Owens, T. J. and G. Zandt (1985). The response of the continental crust-mantle boundary observed on broadband teleseismic receiver functions, *J. Geophys. Res.* 12: 705–708.

Pasyanos, M., W. Walter, and M. Flanagan (2003). Geophysical models for nuclear explosion monitoring, in *Proceedings of the 25th Seismic Research Review—Nuclear Explosion Monitoring: Building the Knowledge Base*, LA-UR-03-6029, Vol. 1, pp.125–134

Pasyanos, M., W. Walter, M. Flanagan, P. Goldstein, and J. Bhattacharyya (2004). Building and testing an a priori geophysical model for western Eurasia and North America, *Pure Appl. Geophys.* 161: 235–281.

Pasyanos, M. (2005). A variable resolution surface wave dispersion study of Eurasia, North Africa, and surrounding regions, *J. Geophys. Res.* 110: doi: 10.1029/2005JB003749.

Schultz, C., S. Myers, J. Hipp, and C. Young (1998). Nonstationary Bayesian kriging: A predictive technique to genereate spatial corrections for seismic detection, location, and identification. *Bull. Seis. Soc. Am*. 88: 1275–1288.

Wilson, D., D. Angus, J. Ni, and S. Grand (2006). Constraints on the interpretation of *S*-to-*P* receiver functions, *Geophys. J. Int*. 165: 969–980.

Wittlinger, G. and V. Farra (2007). Converted waves reveal a thick and layered tectosphere beneath the Kalahari super-craton, *Earth Planet. Sci. Lett*. 254: 404–415.